Anbar Journal of Engineering Science (AJES) **Vol. 17 , No. 1 (2026) , pp. 71 ~ 83**
P-ISSN: 1997-9428 ; E-ISSN: 2705-7440 DOI: http://doi.org/10.37649/AJES.26.0004

University of Anbar

Anbar Journal of Engineering Science

journal homepage: https://ajes.uoanbar.edu.iq/

Numerical Comparative Thermal Analysis of a Parabolic Trough Solar Collector Using Circular, Semi-Oval, and Isosceles Triangular Absorber Tubes

Hassanien Ali Jaber[a], Alaa R. Al-Badri[b]

[a] *Departmen of Mechanical Engineering, College of Engineering, Wasit University, Wasit, Iraq.*
[a]*Email: Std2023203.Hassanien.Ali@uowasit.edu.iq; ORCID: https://orcid.org/0009-0007-8821-1729*
[b] *Departmen of Mechanical Engineering, College of Engineering, Wasit University, Wasit, Iraq.*
[b]*Email: albadria@uowasit.edu.iq; ORCID: https://orcid.org/0000-0002-9904-2360*

PAPER INFO

Paper history
Received: 20/01/2026
Revised: 17/04/2026
Accepted: 13/05/2026

Keywords:
Parabolic Trough Solar Collector
Absorber tube geometry
Temperature distribution
Thermal efficiency
Solar energy

ABSTRACT

This paper presents a numerical comparative study on a parabolic trough solar collector (PTSC) with isosceles triangular, semi-oval, and circular absorber tubes. This study takes into account volumetric water flow rate through the absorber tube. The thermal efficiency of the collector and pressure drop along the absorber tube are determined and adopted for comparison. The results showed that the absorber tube shape has a significant influence on the thermal performance. The thermal efficiency with isosceles triangular, semi-oval, and circular tubes were 54.6%, 53.8%, and 42.3%, respectively. This indicates improvement by 29.1% and 27.2% for the isosceles triangular and semi-oval tubes compared to the circular one. However, the isosceles triangular tube showed penalty in pressure drop compared to the other tubes. The thermal efficiency increased with increasing volumetric flow rate due to the enhancement in convection heat transfer. However, the influence of changing water flow rate on the thermal efficiency was comparatively small. In conclusion, the results of this study can be applied to enhance the thermal performance of present and new designed PTSC by changing the cross-section of the absorber tube.

1. Introduction

The growing worldwide pressure for sustainable energy resources has led to the pursuit of advanced exploration of solar thermal systems design and optimization. Out of all types of technology, parabolic trough solar collectors (PTSCs) are those that gained considerable attention for the application in channeling solar radiation into a receiver tube and thus attain greater thermal efficiency compared to the typical flat-plate collectors. The performance of PTSCs is greatly dependent on various factors such as the geometry and material of the absorber tube, the optical properties of the concentrator, and the working fluid condition. Such a factor in improving the collector's performance is derived from the configuration of the absorber tube, which directly controls the rate of heat transfer from the concentrated solar flux to the working fluid. Traditionally, PTSCs were circular tubes, but other

* Corresponding author: Hassanien Ali Jaber; Std2023203.Hassanien.Ali@uowasit.edu.iq ; +9647710981870

geometries have been developed recently in order to modify the thermal performance. The non-circular shapes allow for increased surface area for heat transfer, change the flow profile, reduce heat loss, and provide better efficiency in overall energy conversion.

Studies have shown that using nanofluids as working fluids within complex absorption tube geometries improves heat transfer by increasing thermal conductivity between nanoparticles, [1-5].

Ghomrassi et al.,[6]The numerical study using SOLTRACE software showed that the solar heat flux on the perimeter of the lower part of the absorber tube increases with increasing diameter of the absorber tube; however, this leads to increased heat loss by radiation. Ye et al.,[7] focused on secondary flow and its effect on thermal behavior in non-uniform heat flows in parabolic trough collectors. Using a simultaneous Monte Carlo Ray Tracing (MCRT) and Finite Volume Method (FVM), tetrahedral protrusions in absorber tubes promoted thermal transfer via 14.6% growth in the Nusselt number and a 7.87× increase in secondary flow intensity, especially in high inlet temperatures. Akhbari et al.,[8] A solar collector channel with a triangular cross-section and a U-shaped airflow pattern was tested. The mass flow rate associated with the highest efficiency was determined. A mathematical model was also developed to predict the solar water heater's performance. The equilateral triangular cross-section demonstrated the highest thermal performance. Kumar et al.,[9] Simulation results using commercial ANSYS software for the triangular duct solar air heater showed a 2.88 increase in Nusselt number and a doubling of the coefficient of friction compared to the non-ribbed duct. Abdel-Hady et al.,[10] the advantages of the glass cover in terms of heat retention, ease of cleaning, and corrosion resistance outweighed the focal deflection of the glass-covered collector, which was more pronounced than in the open collector. Marchini et al.,[11] the study confirmed that while the colour is the primary determining factor for a material's radiative properties, surface texture, particularly roughness and undulation, plays a significant secondary role. Improving surface properties is a promising approach for reducing cooling energy consumption and mitigating the effects of urban heat islands. Mohamad et al.,[12] experimental and theoretical works prove. In high-temperature applications, the cavity receiver design offers potential economic and practical advantages over current technologies. It demonstrates significant advantages in achieving higher operating temperatures and improved thermal efficiency, especially when combined with heated mirror coating and optimised aperture size. Raj et al.,[13] the insertion process significantly increased the pressure drop while improving heat transfer. In comparison to the non-inserted tube, which showed a pressure drop of 45 Pa, the inserted absorption tube showed a pressure drop of 225 Pa. The inlet region had the highest velocity, whereas the outlet region had the lowest. This suggests that the pressure drop had a greater impact on flow velocity than the heat gain from the temperature increase. Venkatesaperumal et al.,[14] showed that, even though the friction factor increases, incorporating a corrugated tube receiver with conical strip inserts greatly improves the heat transfer performance and overall efficiency of solar parabolic trough collectors. Saeed et al.,[15] evaluated parabolic and flat absorber designs in the Middle Eastern irradiance. The double absorption of multi-channel absorber tubes, as used with CuO-water nanofluids, provided a greater heat recovery in the range of solar intensities during the experiment of the present study.

According to this survey, the previous studies did not focus on the influence of tube cross section shape and its effect on the performance of PTSC. Thus, the present study investiges the absorber tube shape by a comparative numerical analysis of the thermal performance with absorbers of circular, semi-oval, and isosceles triangular cross-sections. For all tubes, the total external surface area is kept constant. The investigation encompasses the water heating behavior, heat transfer, and thermal efficiency with respect to volumetric flow rate and sunshine hours.

2. Methodology

Numerical analysis was performed using the Computational Fluid Dynamics (CFD) software within the commercial ANSYS 2022R1 program to study the thermal performance of the absorber tube and predict the potential impact of varying the tube's cross-sectional shape (isosceles triangular, semi-oval, and circular, as reference). The upper part of the tube is assumed to receive direct solar radiation, influenced only by the absorption of its parabolic surface. The lower part, on the other hand, receives concentrated solar radiation reflected from the collector surface, influenced by the collector surface reflection, the absorption of the absorber tube

surface, and the parabolic concentration ratio shown in Fig. 1. Convectional heat losses were neglected due to the presence of a sealed, vacuum-sealed glass envelope, and radiative heat losses were considered negligible [16].

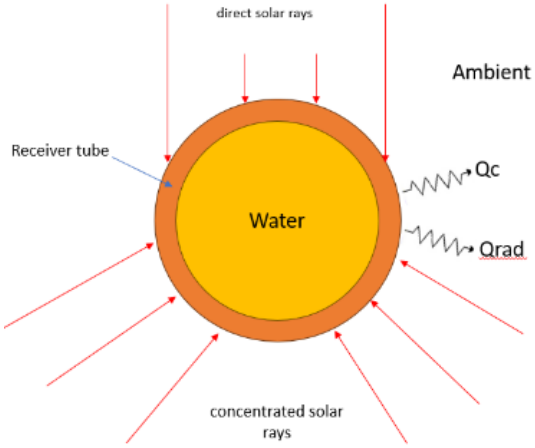

Figure 1: Solar irradiation on the surface of the absorber tube.

A PTSC system was designed for medium-scale thermal applications under the climatic conditions of Al-Hayy town, Wasit Governorate, Iraq. The system consists of two main components: a parabolic trough and an absorption tube, in addition to the PTSC system, as shown in Figure 2.

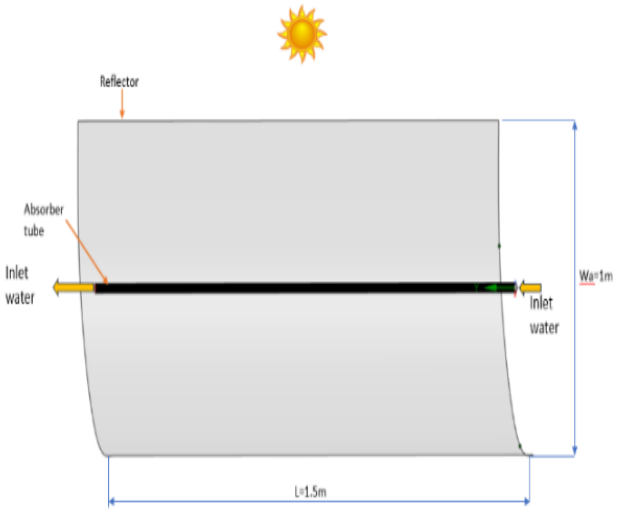

Figure 2: Parabolic Trough Solar Collector (PTCS)

The concentrator was constructed using reflective aluminum sheets shaped into a parabolic profile to maximize solar flux concentration onto the focal line. The main design in Table 1. The parabola was oriented along two axes, and manual solar tracking was performed during the test hours (08:00-16:00). The reflective surface was assumed to be ideal, and optical losses were neglected.

Table 1: Parameters of the collector

Parameter of the collector		Unit
Aperture width	1000	mm
Aperture length	1500	mm
Focal length	250	mm
Rim angle	90	degree
Concentration ratio	14.322	

At the focal line of the parabola, a copper absorber tube was installed to capture and transfer the concentrated solar radiation into the working fluid (water). Copper was selected due to its high thermal conductivity (~385 W/m·K), ease of fabrication, and wide application in solar thermal systemsThree different cross-sectional geometries of absorber tubes were analysed, all with constant external surface area, and were analyzed as a basis for comparison. The dimension of the absorber tube is detailed in Table 2.

Table 2: Dimensions of absorber tubes

Circular section		
dimension		unit
Diameter	22.225	mm
Thick	O.8	mm
length	1500	mm
Semi-Oval section		
Minor radius (a)	11.1125	mm
Major radius (b)	19	mm
Thick	0.8	mm
Length	1500	mm
Isosceles Triangular section		
Base	22.225	mm
Sides	23.58	mm
Thick	0.8	mm
length	1500	mm

All tubes were coated with matte black selective paint to maximize solar absorptivity while reducing reflection losses. The ends of the tubes werethermally insulated to minimize axial heat conduction losses, as shown in Fig. (3).

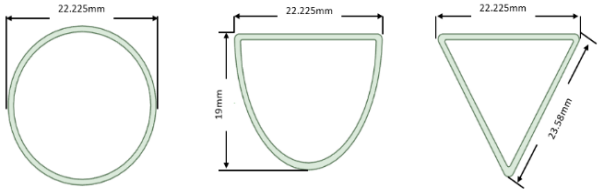

Figure 3: Design of geometric shapes for cross-sections.

Water was selected as the working fluid for its abundance, low cost, and favorable heat capacity. The flow rates were 0.2, 0.3, 0.4, 0.5, 0.6, 0.7, and 0.8 L/min.

Solar radiation intensity data perpendicular to the collector surface were obtained from [17] for 1 November 2025. The ambient temperature and wind speed data wasduring the analysis hours (800-1600) obtained from [18] as shown in Fig.4.

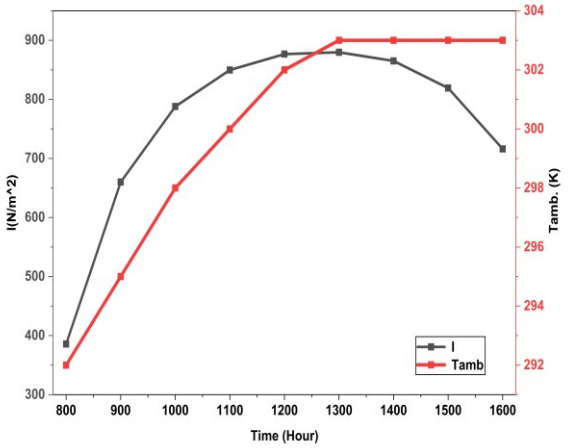

Figure 4: Weather conditions and intensity of direct normal irradiance.

2.1. Boundary coditions

In numerical simulations, the flow is assumed to evolve hydrodynamically and thermally. The properties of the working fluid (water) and the absorber tube material (copper) are assumed to be constant.

(a) Fluid inlet boundary conditions:
The flow is characterized by constant velocity and temperature at the absorber tube inlet of the receiver.
(b) Boundary wall conditions:
Non-slip conditions are applied within the tube wall.
A uniform heat flux is applied to the outer surface of the tube.
(c) The upper part of the absorber tube is exposed to direct solar radiation[19].
(d) The lower part of the receiver is exposed to concentrated solar radiation reflected from the collector surface.
(e) A zero-pressure gradient is applied across the outlet boundary.
(f) The initial conditions are shown in Table (3).

Table 3: Initial conditions

Time[h]	I[W/m²]	Ti[K]
800	385.79	292.00
900	660.2	295
1000	787.9	298
1100	849.9	300
1200	876.7	302
1300	879.9	303
1400	865.3	303
1500	819.2	303
1600	716.1	303

2.2. Processes

Because the heating is uneven on both sides of the outer surface of the absorber tube, the laminar flow characteristics are affected. The velocity profile is no longer a parabola, as in conventional laminar flow [20] Fig. 5 shows the velocity profile with radius for circular tubes. The solution becomes more complex if we consider the non-circular cross-sections studied, such as isosceles triangles and semi-oval. Therefore, the k-ε model was used because it simulates the flow inside the tubes with uneven heating, rather than ideal laminar flow.

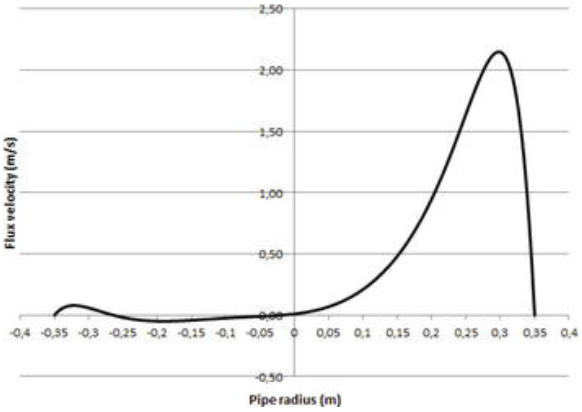

Figure 5. the velocity profile with radius for circular tube

Steady-state modeling of turbulent flow is ensured by solving differential equations expressing continuity, momentum, and energy. A k-ε achievable turbulence model with wall manipulation is used to solve these equations in turbulent flow, as it is more accurate [21]. In fact, for regions near solid walls where viscosity effects predominate over turbulence effects, a near-wall model approach with "enhanced wall manipulation" is used to handle the near-wall regions [22]. The SIMPLE algorithm has been used to enable pressure-velocity coupling [23]. All second-order equations were applied to each of pressure,

momentum, turbulent kinetic energy, turbulent dissipation rate, and energy.

2.3. Governing equations:

The general equations governing steady-state continuity, momentum, and energy using CFD are as follows[21]:

Continuity equation:

$$\frac{\partial}{\partial x_i}(\rho u_i) = 0 \quad (1)$$

Momentum equation:

$$\frac{\partial}{\partial x_i}(\rho u_i u_j) = -\frac{\partial P}{\partial x_i} + \frac{\partial}{\partial x_j} * \left[(u_{i+} u_j) \left(\frac{\partial u_i}{\partial x_j} + \frac{\partial u_i}{\partial x_i} \right) - \frac{2}{3} * (\mu + \mu_t) \frac{\partial u_l}{\partial x_l} \delta_{ij} \right] \quad (2)$$

Energy equation:

$$\frac{\partial}{\partial x_j}(\rho u_j T) = \frac{\partial}{\partial x_j}\left[\left(\frac{\mu}{Pr} + \frac{\mu_t}{\sigma_t} \right) \frac{\partial T}{\partial x_j} \right] \quad (3)$$

k equation:

$$\frac{\partial}{\partial x_j}(\rho u_j k) = \frac{\partial}{\partial x_j}\left[\left(\mu + \frac{\mu_t}{\sigma_k} \right) \frac{\partial k}{\partial x_j} \right] + P_k - \rho\varepsilon \quad (4)$$

ε equation:

$$\frac{\partial}{\partial x_j}(\rho u_i \varepsilon) = \frac{\partial}{\partial x_j}\left[\left(\mu + \frac{\mu_t}{\sigma_\varepsilon} \right) \frac{\partial \varepsilon}{\partial x_j} \right] - \rho C_{\varepsilon 2} \frac{\varepsilon^2}{K} + C_{\varepsilon 1} \frac{\varepsilon}{k} P_k \quad (5)$$

Where the Turbulence viscosity:

$$\mu_t = C_\mu \rho \frac{k^2}{\varepsilon} \quad (6)$$

And the production rate of k:

$$P_k = \mu_t \frac{\partial u_i}{\partial x_i}\left(\frac{\partial u_i}{\partial x_j} + \frac{\partial u_i}{\partial x_i} \right) \quad (7)$$

In the above equations, u is the velocity; P is the pressure; $\delta$is denotes Kronecker's delta; T is the thermodynamic temperature; Pr is the turbulent Prandtl number; k and ε are the turbulent kinetic energy and turbulent dissipation rate, respectively; σ_k and σ_ε are the turbulent Prandtl numbers for diffusion of k and ε, respectively; C_μ , $C_{\varepsilon 1}$ and $C_{\varepsilon 2}$ are the corresponding coefficients in the turbulence.

The thermal performance of the PTSC can be described by applying the fundamental principles of conservation of energy and heat transfer to the absorber tube and the working fluid. The difference between absorbed solar energy and the associated heat losses determines the net useful energy gained by the working fluid:

$$Q_u = Q_{abs} - Q_{loss} \quad (8)$$

The absorbed solar energy is a function of incident solar irradiance, optical properties, and geometric factors of the collector [19]:

$$Q_{abs} = (I * \tau_g * A_{up} * \alpha_a) + (I * \tau_g * A_{bo} * C_r * \alpha_a * \rho_c) \quad (9)$$

where: A_{up}, A_{bo} are the surface area of the upper and lower parts, respectively,τ_g is transmittance of a glass cover =1, α_a is the absorptivity of the tube surface =0.9, ρ_c is the reflectivity of the parabolic surface =0.85, C_r is the concentration ratio=14.32. The surface area of the circular tube is calculated using the following relationship:

$$A_{up\text{-}c} = A_{bo\text{-}c} = \frac{1}{2}(\pi * D_O) * L \quad (10)$$

The surface areas of non-circular tubes are calculated using the following relationships:

$$A_{up} = D_O * L \quad (11)$$

$$A_{bo} = (\pi - 1) * D_O * L \quad (12)$$

The PTSC concentration ratio was calculated using the relationship [22]

$$C_r = \frac{W_a}{(\pi * D_O)} \quad (13)$$

The useful heat gain is determined from the fluid temperature rise across the tube [24, 25]:

$$Q_u = \dot{m} C_p (T_o - T_i) \quad (14)$$

Heat loss mechanisms include convection and radiation from the outer surface of the absorber tube to the ambient environment:

$$Q_{loss} = Q_{conv} + Q_{rad} \quad (15)$$

Convective heat loss:

$$Q_{conv} = h_c A_s (T_w - T_a) \quad (16)$$

Radiative heat loss:

$$Q_{rad} = \varepsilon_s \sigma A_s \left(T_w^4 - T_{asky}^4 \right) \quad (17)$$

Where: A_s is the outer surface area of the tube, $\varepsilon_s$is the emissivity of the absorber tube surface. The ambient temperature T_a and the sky temperature T_{sky} are connected in the following way [25]:

$$T_{sky} = 0.0552 * T_a^{1.5} \quad 18$$

The instantaneous thermal efficiency is expressed as [25, 27]:

$$\eta = \frac{Q_u}{Q_s} \quad 19$$

This represents the ratio of useful heat transferred to the fluid to the total solar energy incident on the collector aperture.

$$Q_s = I * A_{aperture} \quad 20$$

Where: I is direct normal irradiance and $A_{aperture}$ is solar collector opening area.

The flow state inside the absorption tube is characterized by the Reynolds number, where its limits were (205.5 - 821.9) with a volumetric flow rate of (0.2 - 0.8) L/min through the circular tube, while its limits were (245.7 - 982.9) and (313.6 - 1254.3) for the semi-oval and isosceles triangular tubes, respectively, with the same mass flow rate due to the change in hydrodynamic diameter resulting from the change in the cross-sectional shape of the non-circular tubes, and it is calculated from the relationship:

$$Re = \frac{4 * \dot{m}}{\pi * D_h * \mu_f} \quad 21$$

Where: $\dot{m}$is mass flow rate, D_h is hydraulic diameter, μ_f is the dynamic viscosity of water. For non-circular cross-sections, the hydraulic diameter is given by:

$$D_h = \frac{4A_c}{P_w} \quad 22$$

Where: A_c is the cross-sectional flow area, P_w is the wetted perimeter.

The mass flow rate calculated by:

$$\dot{m} = \frac{\rho_f * V^{\circ}}{60 * 1000} \quad 23$$

Where: ρ_f is working fluid density in kg/m³,V° is volumetric flow rate in L/min.

The percentage of enhancement in thermal efficiency of non-circular absorber tubes compared to circular absorber tubes is calculated using the following relationship:

$$\frac{\eta_{non_{cir.}}}{\eta_{cir.}}\% = \frac{\eta_{non_{cir.}} - \eta_{cir.}}{\eta_{cir.}} * 100\% \quad 24$$

Where: η_{cir} is thermal efficiency of PTC using a circular tube and $\eta_{non_{cir.}}$ is thermal efficiency of PTC using anon-circular tube.

2.4. Validation result

To validate the results of the ANSYS Fluent program, the experimental results of [27] were compared with a simulation of the same conditions in terms of inlet temperature, volumetric water flow rate, solar radiation intensity, PTSC dimensions, and absorption tube. As shown in fig.6. The deviation was 5.2%, which is quite acceptable in this study given the neglect of heat loss. The dimensions of PTSC are shown in the table 4 at solar irradiant intensity 1024 W/m² and water inlet temperature at 36,3 C°.

Table 4. PTSC dimensions of [27]

Dimension	Value	Unit
Aperture width	1000	mm
Length	1000	mm
Focal length	250	mm
Do	15	mm
Di	13	mm

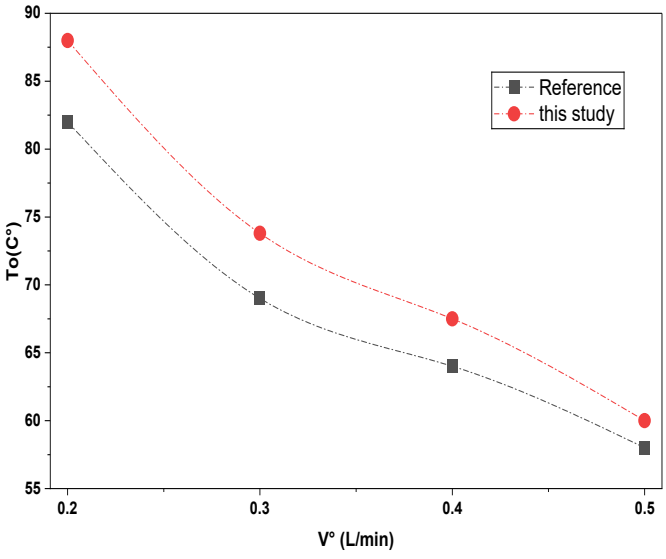

Figure 6. Comparing experimental results of [27] with ANSYS simulations

3. Results and discussion

3.1. Mesh Independence

An exhaustive volume was employed in ANSYS Fluent to discretize the computational domain representing the absorber tube geometries (Circular, Isosceles Triangular, and Semi-Oval cross-sections). A structured/unstructured mesh was generated, with sufficient refinement near the tube walls to obtain an accurate measurement of the thermal boundary layer and velocity gradients. Skewness and orthogonality of the meshes were verified, and all the meshes remained within recommended quality limits for numerical stability and accuracy. A mesh-independence study was done to verify that numerical results were independent of the mesh size. Different mesh densities were tested for each tube geometry, and the exit fluid temperature and useful heat gain were monitored as optimization progressed. It was observed that after a certain number of elements, the differences between predictions became minimal (<0.1%), indicating convergence of the mesh shown in Fig. 6. Therefore, the final mesh with 2562705 elements was chosen for the circular tube, and 1832772 and 2056875 elements were chosen for the isosceles triangle and semi-oval tubes, respectively, with deviation percentages of <0.1% and <0.1%, respectively, as a compromise between computational accuracy and efficiency. Fig. 7 explains mesh domains.

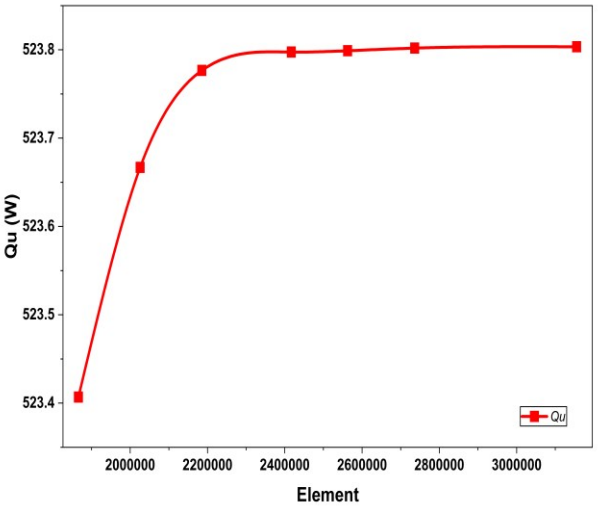

Figure 7. Mesh-Independence.

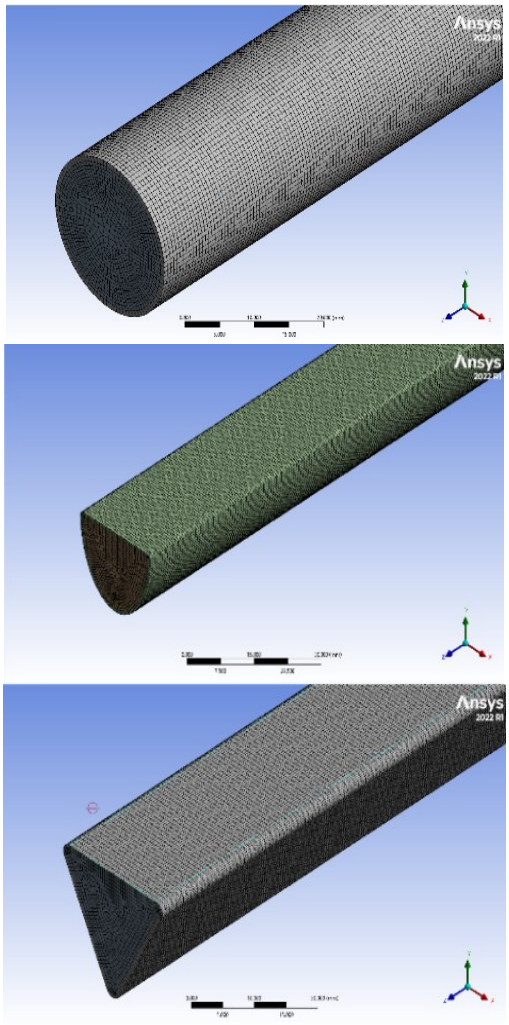

Figure 8: Mesh domains

3.2. Thermal performance analysis results

Here, the results report the thermal performance of a parabolic trough solar collector with Circular, Semi-Oval, and Isosceles Triangular absorber tube geometry. The analysis starts out using the variation of solar irradiance and ambient temperature for the entire operating period (08:00–16:00), which directly determines the amount of solar energy available for conversion. Then, the heating profiles of water under the three absorber geometries are compared, and subsequently, the useful thermal energy gained and thermal efficiencies obtained are measured. Finally, contour plots, based on ANSYS simulations, are presented to show the temperature distribution along the tubes, providing further physical data on heat transfer mechanisms in the different geometries. This joint approach allows a total view of the impact of

absorber cross-section on the overall performance of the parabolic trough collectors.

Fig.8 illustrates the change in water temperature exiting the tubes during periods of intense solar exposure on November 1, 2025. The water temperature gradually increases from 8:00 to 13:00 h, reaching its peak, and then slowly decreases until 16:00 h. This is due to variations in the intensity of solar radiation incident perpendicularly on the mobile surface during the incubation period. Higher outlet temperatures were observed for the tubes with isosceles triangular and semi-oval cross-sections, reaching 323.6 K and 323.3K, respectively, compared to the exit temperature of the conventional circular tube, which reached 319 K during peak solar radiation hours, with a flow rate of 0.5 L/min.

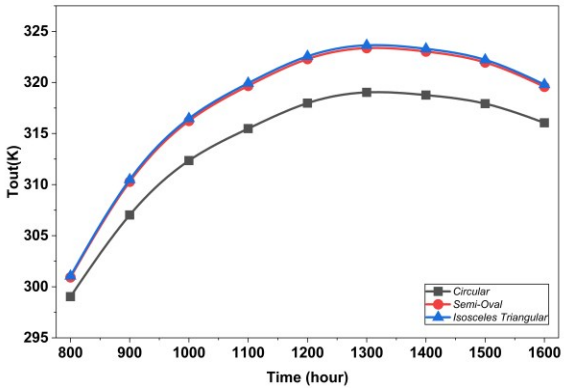

Figure 9: The water outlet temperature changes with hours of exposure to sunlight with tubes.

Fig. 9 shows how thermal efficiency is affected by changes in flow rate through tubes with isosceles triangular, semi-oval, and circular cross-sections. A very slight increase in thermal efficiency is observed with increasing volumetric water flow rate for all tubes. On the other hand, the isosceles triangular tube exhibits the highest efficiency at all flow rates. It is followed closely behind by the semi-oval tube, driven by increases in the surface area-volume ratio and the surface area receiving concentrated solar radiation, and then the circular tube. The efficiencies reached 55.6% for the isosceles triangular shape, 54.5% for the semi-oval shape, and 42.8% for the circular shape under the same simulated conditions at the peak solar radiation hours, with a flow rate of 0.8 L/min.

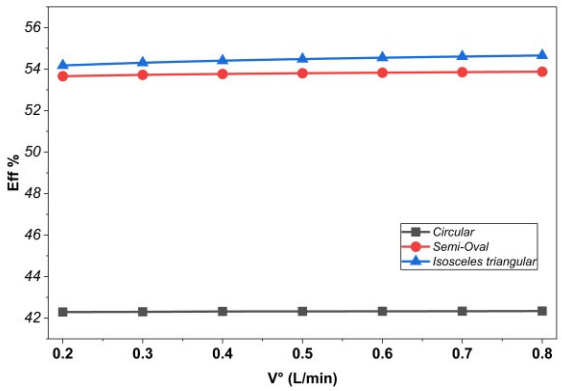

Figure 10: The efficiencies with volumetric flow rate through tubes.

Fig.10 shows the temperature distribution across the tube outlet at a flow rate of 0.5 L/min and a direct solar irradiance of 879.9 W/m² at the peak hour of 13:00, where an increase in outlet temperatures is observed. This is due to an increase in the surface area of the tube receiving concentrated solar radiation reflected from the collector surface, at the expense of the surface receiving direct solar radiation in the isosceles triangle and semi-oval shapes. The isosceles triangle is characterized by sharp angles that cause disturbances, which enhance convection heat transfer within the tube.

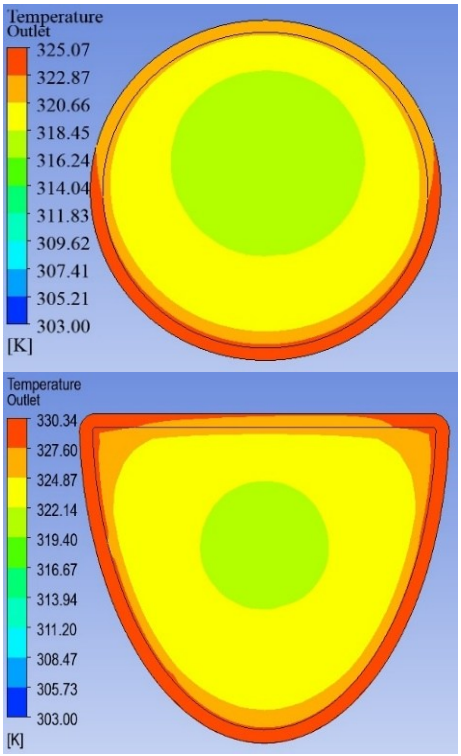

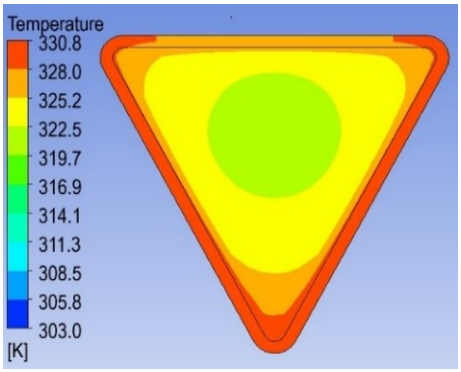

Figure 11: Temperature contours at the outlet of tubes.

Fig. 11 shows the temperature distribution along isosceles triangular, semi-oval, and circular absorber tubes located at the focal line of a parabolic trough collector. Contour lines show the inlet water temperature at 303 K (blue area), which gradually approaches 330.8 K and 330.34 K at the outlet of the isosceles triangular and semi-oval tubes, respectively, and 325.07 K at the outlet, at a flow rate of 0.5 L/min and a direct solar irradiance of 879.9 W/m² at the peak hour of 13:00. Isosceles triangular and semi-oval shapes offer a larger effective surface area because the surface area of the lower section receiving concentrated solar radiation is greater than in a circular tube, thus contributing to increased heat transfer areas compared to a conventional circular tube. Since the surface area to volume ratio is higher for an isosceles triangular tube than for a circular tube and also higher for a semi-oval tube than for a circular tube, the increased water velocity through the tube and the sharp angles of non-circular tubes result in increased convection heat transfer between water layers due to internal turbulence. This suggests that non-circular geometries may improve the performance of parabolic trough solar collectors.

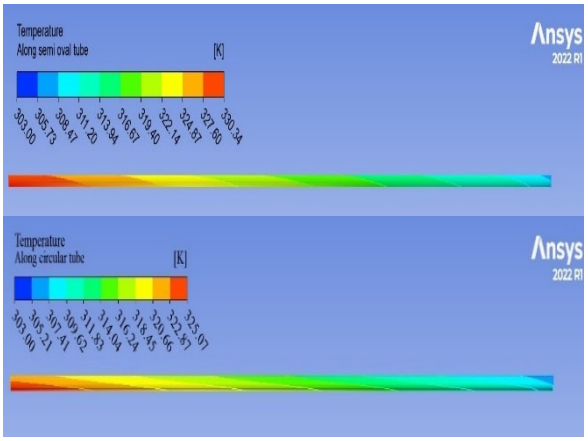

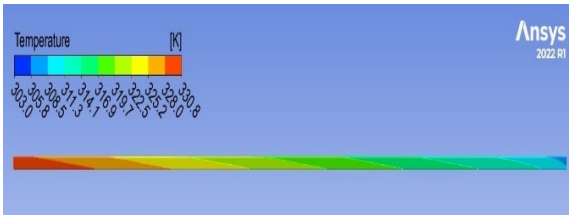

Figure 12: Temperature contours at along of tubes.

Fig.12 illustrates the change in the convective heat transfer coefficient of the working fluid (water) wall in contact with the inner tube surface as the flow rate changes through isosceles triangular, semi-oval, and circular (as a reference) absorption tubes at a direct solar irradiance of 879.9 W/m² at peak time 13:00. A gradual, non-linear increase in the convective heat transfer coefficient was observed with increasing volumetric flow rate across the three tube shapes. The convective heat transfer coefficient was particularly high in the isosceles triangular, and semi-oval shapes, reaching 274 (W/m²*K) and 271.9 (W/m²*K), respectively, while it was 236.3 (W/m²*K) for the circular tube. This is because the cross-sectional area of non-circular tubes is less than that of circular pipes, even though the wetted perimeter of all pipes is the same, in addition to the presence of sharp angles that impede the flow of water through the tube.

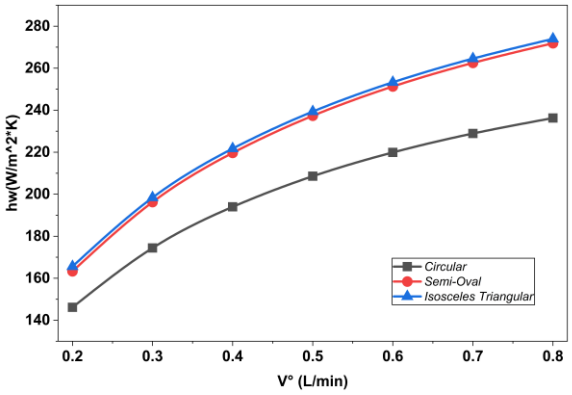

Figure 13: The convection heat transfer coefficient of water changes with the volumetric flow rate through tubes of different cross-sections.

Fig.13 shows the change in working fluid (water) pressure drop between the tube inlet and outlet as the flow rate changes through isosceles triangular, semi-oval, and circular (as a reference) absorption tubes. A gradual, non-linear increase in the pressure drop was observed with increasing volumetric flow rate across the three tube shapes. The pressure drop

was significantly higher in the isosceles triangular tube, reaching 35.6 Pa, compared to 19.2 Pa for the semi-oval shape and 12.3 Pa for the conventional circular shape at a flow rate of 0.8 L/min and peak solar radiation hours. This is attributed to the increased impedance resulting from the increased water velocity caused by the change in the cross-sectional shape of the two non-circular tubes. This impedance also acts as a disturbance even at low water velocities.

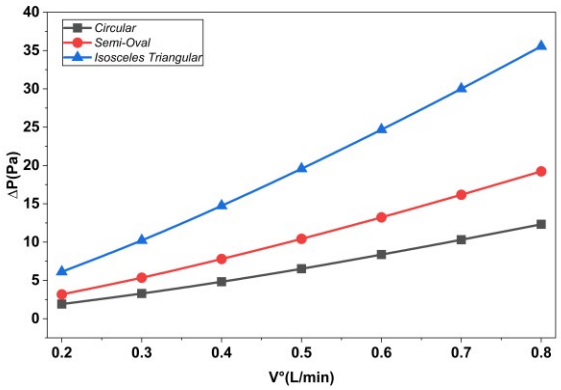

Figure 14: The pressure drops through tubes change with the volumetric flow rate.

4. Conclusion

In this study, a numerical comparative study was conducted using the ANSYS software for a parabolic trough solar collector, using inverted isosceles triangular, inverted semi-oval, and conventional circular absorber tubes as. The effect of increasing the volumetric water flow rate through the absorber tubes on the solar collector's thermal efficiency was investigated. The effect of increasing the flow rate on thermal efficiency was small, as the thermal efficiency increased with increasing volumetric flow rate due to the increased convection of the water. However, the effect of changing the cross-sectional shape of the absorber tube, while maintaining the total surface area of the tube, was significant. Under the same simulated conditions, the inverted isosceles triangular and inverted semi-oval shapes achieved thermal efficiencies of 54.6% and 53.8%, respectively, while the circular shape achieved 42.3%. The percentage improvement in thermal efficiency was 29.1%, 27.2% for the inverted isosceles triangular and inverted semi-oval shapes, respectively. This improvement was due to an increased surface area to volume ratio and a larger surface area of the tube receiving concentrated solar radiation reflected from the collector surface, at the expense of the surface area of the tube receiving direct solar radiation. The inverted isosceles triangular shape offers a slight advantage due to its sharp angles and flat walls, which enhance heat transfer but result in a greater pressure drop, making this geometry the best choice for improving the efficiency of parabolic trough solar collectors with high irradiance zones. Considering its simplicity and stable flow, the semi-oval tube may represent a viable alternative compared to the circular tube, which remains a reference only. Finally, the results of this study can be applied to enhance the thermal performance of PTCs by changing the cross-section of the absorber tube.

Nomenclature

Q_u	Useful thermal energy (W)
Q_{abs}	The absorbed solar energy(W)
Q_{loss}	The losses in thermal energy(W)
I	Direct normal irradiance (W/m²)
$A_{up\text{-}c}$	Outer surface area of the upper part of the circular tube (m²).
A_{up}	Outer surface area of the upper part of the isosceles triangular and semi-oval tube (m²).
$A_{bo\text{-}c}$	Outer surface area of the bottom part of the circular tube (m²).
A_{bo}	Outer surface area of the upper part of the isosceles triangular and semi-oval tube (m²).
C_r	The solar collector concentration ratio =14.322.
W_a	Parabolic trough opening width =1m.
D_O	Outer diameter of absorber tube=0.022225m.
L	Length of absorber tube and collector=1.5m.
$\dot{m}$	Mass flow rate of the fluid (kg/s).
V°	Volumetric flow rate in L/min.

c_p	Specific heat of water ($J/kg \cdot K$).
T_o, T_i	Outlet and inlet fluid temperatures (K)
Q_{conv}	Convective heat loss(W)
Q_{rad}	Radiative heat loss(W)
h_c	Convective heat transfer coefficient of air$(W/(m^2 \cdot K))$.
A_s	External surface area of the absorber tube (m^2).
T_w	Surface wall temperature of the absorber tube (K)
T_a	Ambient temperature (K)
T_{sky}	The sky temperature(K)
$A_{aperture}$	Solar collector opening area (m^2)
$\bar{V}_f$	Mean velocity of the fluid (m/s)
D_h	Hydraulic diameter of the tube (m)
A_c	The cross-sectional flow area (m^2)
P_w	The wetted perimeter (m)
Nu	Nusselt number (dimensionless)
Re	Reynolds number
Pr	Prandtl number
u	velocity
h_f	Convective heat transfer coefficient of working fluid inside $(W/(m^2 \cdot K))$.
k_f	Thermal conductivity of the working fluid $(W/m \cdot K)$.

Greek symbols

ρ_c	Reflectivity of the parabolic surface =0.85
α_a	Absorptivity of the tube surface =0.9
τ_g	Transmittance of any glass =1
ε_s	Emissivity of the absorber surface =0.32
σ	Stefan-Boltzmann constant = $5.67 \times 10^{-8}(W/(m^2 \cdot K^4)$
ρ_f	The density of water (kg/m^3).
μ_f	The dynamic viscosity of water (Pa*s)
η_{cir}	Thermal Efficiency of the Collector with circular tube.
$\eta_{non_{cir.}}$	Thermal Efficiency of the Collector with non-circular tube.

Reference

[1] Y. Menni, A. J. Chamkha, G. Lorenzini, N. Kaid, H. Ameur, and M. Bensafi, "Advances of nanofluids in solar collectors - a review of numerical studies," *Mathematical Modelling of Engineering Problems*, vol. 6, no. 3, pp. 415–427, Sep. 2019, doi: 10.18280/mmep.060313.

[2] Y. Menni, A. J. Chamkha, and A. Azzi, "Nanofluid flow in complex geometries—A review," 2019, *American Scientific Publishers*. doi: 10.1166/jon.2019.1663.

[3] Z. Sarbazi and F. Hormozi, "Optimization of thermal and hydraulic performance of nanofluids in a rectangular miniature-channel with various fins using response surface methodology," *J. Therm. Anal. Calorim.*, vol. 137, no. 3, pp. 711–733, 2019, doi: 10.1007/s10973-018-7981-5.

[4] Z. Said *et al.*, "Sustainable Thermal Solutions: Enhancing Heat Transfer with Turbulators and Nanofluids," May 01, 2025, *Wiley-VCH Verlag*. doi: 10.1002/aesr.202400335.

[5] E. Barati, A. Sarviha, and M. A. Karamad, "Enhancing solar heater performance: A comprehensive study on hybrid nanofluids and angled-rib turbulators for improved heat transfer and reduced irreversibility," *Next Energy*, vol. 2, p. 100050, Jan. 2024, doi: 10.1016/J.NXENER.2023.100050.

[6] A. Ghomrassi, H. Mhiri, and P. Bournot, "Numerical study and optimization of

parabolic trough solar collector receiver tube," *Journal of Solar Energy Engineering, Transactions of the ASME*, vol. 137, no. 5, Oct. 2015, doi: 10.1115/1.4030849.

[7] M. Ye, W. Gu, Y. Hou, X. Xiang, and J. Liu, "Secondary flow characteristics and their relationship with thermal performance inside the absorber under non-uniform heat flux," *Discover Applied Sciences*, vol. 7, no. 1, p. 74, 2025, doi: 10.1007/s42452-025-06483-7.

[8] M. Akhbari, A. Rahimi, and M. S. Hatamipour, "Modeling and experimental study of a triangular channel solar air heater," *Appl. Therm. Eng.*, vol. 170, p. 114902, Apr. 2020, doi: 10.1016/J.APPLTHERMALENG.2020.114902.

[9] R. Kumar, V. Goel, and A. Kumar, "Investigation of heat transfer augmentation and friction factor in triangular duct solar air heater due to forward facing chamfered rectangular ribs: A CFD based analysis," *Renew. Energy*, vol. 115, pp. 824–835, Jan. 2018, doi: 10.1016/J.RENENE.2017.09.010.

[10] F. Abdel-Hady, S. Shakil, M. Hamed, A. Alzahrani, and A. H. Mazher, "Design, simulation and manufacturing of an integrated composite material parabolic trough solar collector," *International Journal of Engineering and Technology*, vol. 8, no. 5, pp. 2333–2345, 2016, doi: 10.21817/ijet/2016/v8i5/160805005.

[11] F. Marchini, C. Fabiani, L. Latterini, and A. L. Pisello, "Optimising surface morphology for enhanced radiative properties in thermal energy-efficient materials," *Mater. Today Energy*, vol. 45, Oct. 2024, doi: 10.1016/j.mtener.2024.101660.

[12] K. Mohamad and P. Ferrer, "Thermal performance and design parameters investigation of a novel cavity receiver unit for parabolic trough concentrator," *Renew. Energy*, vol. 168, pp. 692–704, May 2021, doi: 10.1016/J.RENENE.2020.12.089.

[13] R. T. K. Raj, T. Srinivas, M. Natarajan, K. A. Kumar, A. Chengappa, and A. Deoras, "Experimental and numerical analysis using CFD technique of the performance of the absorber tube of a solar parabolic trough collector with and without insertion," in *2013 International Conference on Energy Efficient Technologies for Sustainability*, 2013, pp. 550–556. doi: 10.1109/ICEETS.2013.6533444.

[14] R. Venkatesaperumal *et al.*, "Heat Transfer Studies on Solar Parabolic trough Collector Using Corrugated Tube Receiver with Conical Strip Inserts," *Sustainability (Switzerland)*, vol. 15, no. 1, Jan. 2023, doi: 10.3390/su15010378.

[15] F. Saeed, T. Maatallah, A. Houcine, A. Jamal, and S. Ali, "Novel Cooling Strategy for a Hybrid Photovoltaic/Parabolic Dish Concentrator," *Applied Sciences (Switzerland)*, vol. 14, no. 1, Jan. 2024, doi: 10.3390/app14010168.

[16] X. Zhu, L. Zhu, and J. Zhao, "Wavy-tape insert designed for managing highly concentrated solar energy on absorber tube of parabolic trough receiver," *Energy*, vol. 141, pp. 1146–1155, 2017, doi: 10.1016/j.energy.2017.10.010.

[17] "Solar Radiation Data (SoDa) - Energymeteorology." Accessed: Mar. 04, 2026. [Online]. Available: https://energymeteorology.info/data-source/helioclim3-soda/

[18] "Local Weather Forecast, News and Conditions | Weather Underground." Accessed: Mar. 04, 2026. [Online]. Available: https://www.wunderground.com/

[19] K. Ravi Kumar and K. S. Reddy, "Thermal analysis of solar parabolic trough with porous disc receiver," *Appl. Energy*, vol. 86, no. 9, pp. 1804–1812, Sep. 2009, doi: 10.1016/j.apenergy.2008.11.007.

[20] M. Alarcón, M. Seco-Nicolás, J. Pedro Luna-Abad, and A. P. Ramallo-González, "Forced Laminar Flow in Pipes Subjected to Asymmetric External Conditions: The

HEATT© Platform for Online Simulations," in *Pipeline Engineering - Design, Failure, and Management*, IntechOpen, 2023. doi: 10.5772/intechopen.107215.

[21] L. Dou, B. Ding, Q. Zhang, G. Kou, and M. Mu, "Numerical investigation on the thermal performance of parabolic trough solar collector with synthetic oil/Cu nanofluids," *Appl. Therm. Eng.*, vol. 227, p. 120376, Jun. 2023, doi: 10.1016/J.APPLTHERMALENG.2023.120376.

[22] A. A. Hachicha, "Numerical modelling of a parabolic trough solar collector," Universitat Politècnica de Catalunya, 2013. doi: 10.5821/dissertation-2117-95129.

[23] E. Bellos, C. Tzivanidis, and D. Tsimpoukis, "Multi-criteria evaluation of parabolic trough collector with internally finned absorbers," *Appl. Energy*, vol. 205, pp. 540–561, Nov. 2017, doi: 10.1016/j.apenergy.2017.07.141.

[24] B. Stanek, J. Ochmann, D. Węcel, and Ł. Bartela, "Study of Twisted Tape Inserts Segmental Application in Low-Concentrated Solar Parabolic Trough Collectors," *Energies (Basel).*, vol. 16, no. 9, May 2023, doi: 10.3390/en16093716.

[25] J. hu Gong *et al.*, "Improving the performance of a 2-stage large aperture parabolic trough solar concentrator using a secondary reflector designed by adaptive method," *Renew. Energy*, vol. 152, pp. 23–33, Jun. 2020, doi: 10.1016/j.renene.2020.01.019.

[26] E. Bellos and C. Tzivanidis, "Investigation of a star flow insert in a parabolic trough solar collector," *Appl. Energy*, vol. 224, pp. 86–102, Aug. 2018, doi: 10.1016/j.apenergy.2018.04.099.

[27] A. Özcan, A. G. Devecioğlu, and V. Oruç, "Experimental and numerical analysis of a parabolic trough solar collector for water heating application," *Energy Sources, Part A: Recovery, Utilization and Environmental Effects*, vol. 44, no. 2, pp. 4184–4203, 2022, doi: 10.1080/15567036.2021.1924317.